Supplementary material for

Laboratory study of the breaking and energy distribution of internal solitary waves over a ridge

Yulin Guo[1], Xu Chen[1*], Qun Li[2] and Jing Meng[1]

[1] Key Laboratory of Physical Oceanography, Ocean University of China and Qingdao National Laboratory for Marine Science and Technology, Qingdao, China.

[2] MNR Key Laboratory for Polar Science, Polar Research Institute of China, Shanghai, China.

Contents of this file

Text S1. PIV analysis error

Reference Thielicke (2014) to estimate the magnitude of errors for the PIV analysis. In the case of ISW shoaling and breaking, the error is mainly attributable to enhanced flow shear at the interface and bottom boundary. For the largest velocity gradients in the large-region experiment (10 1/s, 0.20 pixels/pixel), the bias error (ε_{bias}) is approximately 0.040 pixel, and the random error (ε_{rms}) is approximately 0.20 pixel. The velocity at the lower layer channel is approximately 0.16 m/s (5.31 px/frame). Therefore, the relative errors of flow velocity are 0.8% and 3.8% for ε_{bias} and ε_{rms}, respectively. For high-resolution experiments, referring to the above method ε_{bias} and ε_{rms} are approximately 0.020 pixel and 0.10 pixel, respectively. The relative errors of flow velocity are 0.2% and 0.9% for ε_{bias} and ε_{rms}, respectively. The discussions of errors is based on the results of Thielicke (2014) with the final interrogation area of 16×16 pixels, and using larger interrogation areas (24×24 pixels in the large-region experiment and 20×20 pixels in the high-resolution experiment) will further increase the accuracy (Raffel *et al.* 2018).

Reference:

RAFFEL, M., WILLERT, C. E., SCARANO, F., KÄHLER, C. J., WERELY, S. T. & KOMPENHANS, J. 2018 *Particle Image Velocimetry – A Practical Guide*. Springer.

THIELICKE, W. 2014 The flapping flight of birds: analysis and application. PhD thesis, University of Groningen.

Text S2. Background oriented schlieren

The background schlieren technique was used to identify the interface to obtain the ISW waveforms and propagation characteristics on a flat bottom. Figure S1 illustrates the relationship between the background stripe and density profiles. Figure S2 shows the whole waveform identified by schlieren. The camera pixel resolution is 0.5 mm. According to Dalziel *et al.* (2007), the smallest variation in N^2 that could be measured is 0.15 $1/s^2$ (which causes a 1 pixel displacement of the stripes). The uncertainty in the measurement depends on the identification of the stripes, e.g., variations in the thickness and degree of distortion of the stripes will affect the accuracy of the identification.

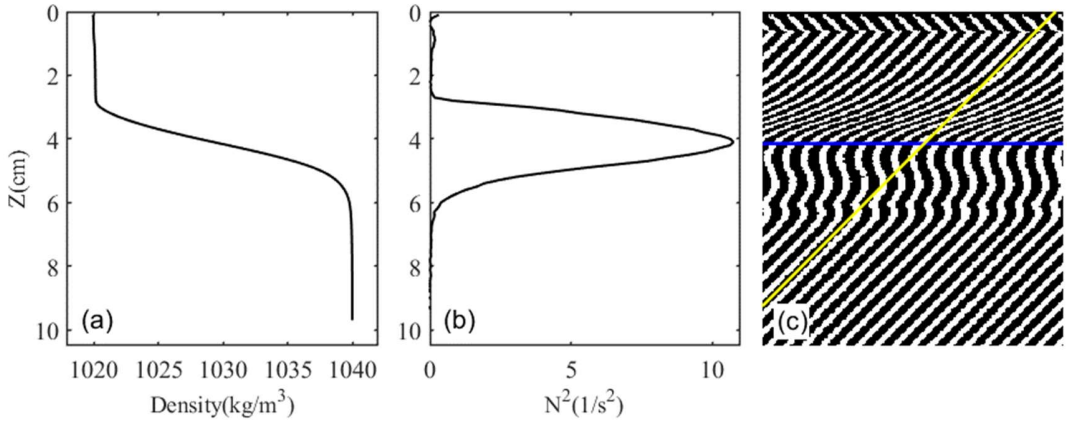

Figure S1. The relationship between the background stripe and density profiles. (a) Density profiles. (b) Buoyancy frequency profiles. (c) Background stripe (45°) vertical position corresponding to (a) and (b). The blue line is the vertical position of the maximum buoyancy frequency, and the yellow line is 45°.

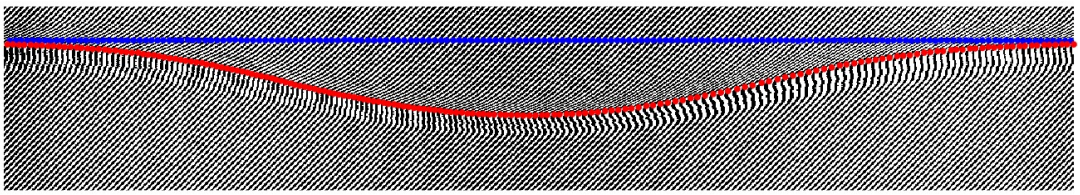

Figure S2. Schematic of the waveform (red dots) and initial interface (blue dots), with 45° lines in the background.

Reference:

DALZIEL, S.B., CARR, M., SVEEN, J.K. & DAVIES, P.A. 2007 Simultaneous synthetic schlieren and PIV measurements for internal solitary waves. *Meas. Sci. Technol.* 18 (3), 533–547.

Text S3. Types of wave-ridge interactions

The following Figure S3 to illustrate the types of breaking and interaction. Includes fission, transition, plunging breaking, collapsing-plunging breaking, transmission and reflection.

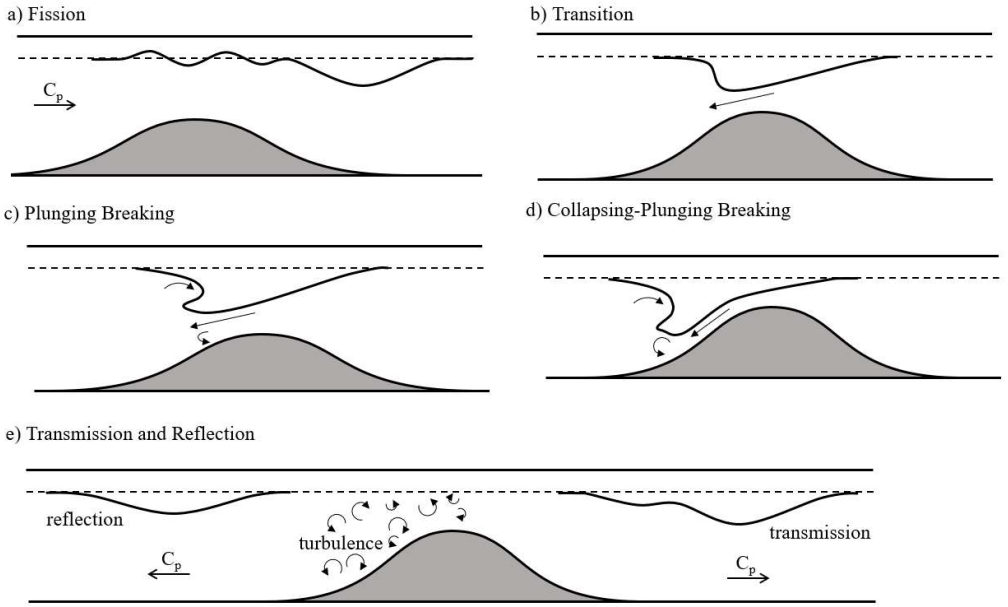

Figure S3. Schematics illustrating different breaking mechanisms (the types of interaction) for wave-ridge interaction.

The evolution process of fission, transition, plunging breaking, and plunging-collapsing breaking is provided Figure S4-S7.

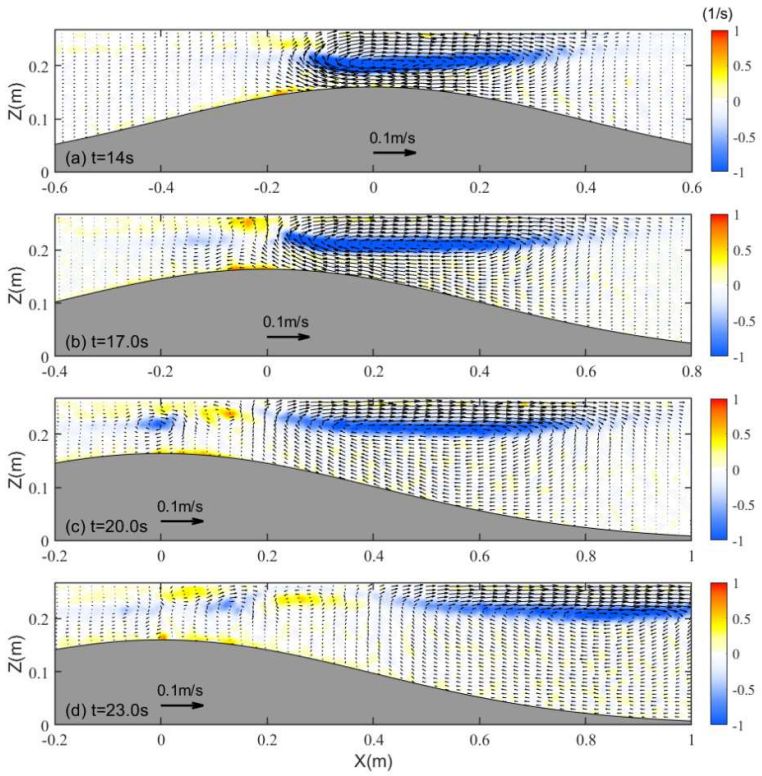

Figure S4. Fission, h_1=0.04 m, h_2=0.24 m, s=0.20, a=0.040 m, ζ=0.65, Ir=0.65.

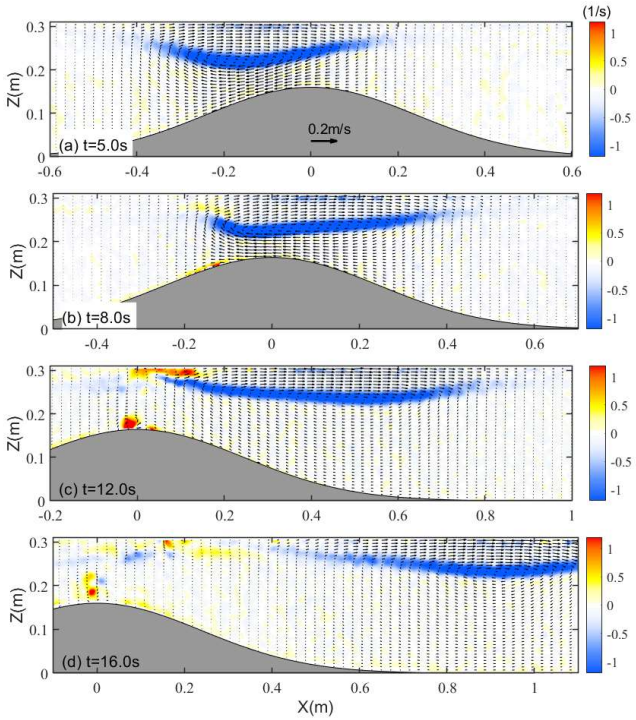

Figure S5. Transition, h_1=0.04 m, h_2=0.28 m, s=0.33, a=0.055 m, ζ=0.58, Ir=0.95.

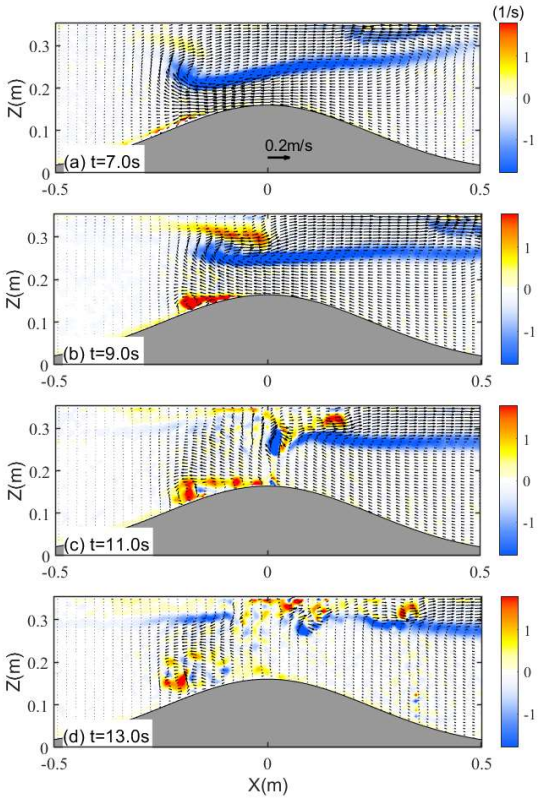

Figure S6. Plunging breaking, h_1=0.04 m, h_2=0.32 m, s=0.33, a=0.092 m, ζ=0.63, Ir=0.82.

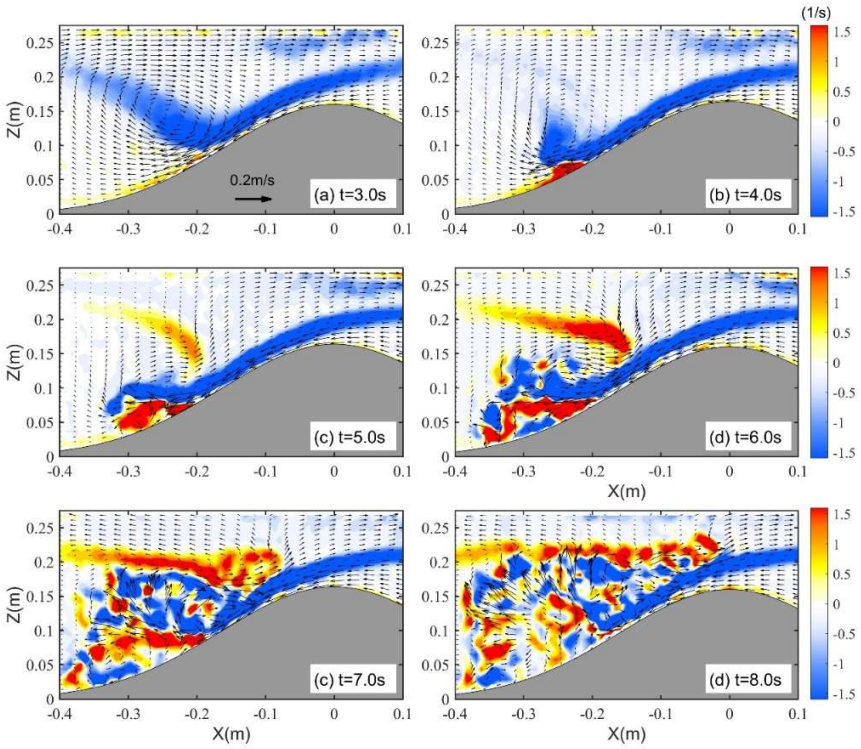

Figure S7. Plunging-collapsing breaking, h_1=0.04 m, h_2=0.24 m, s=0.50, a=0.075 m, ζ=0.91, Ir=1.30.

Text S4. The time scale of breaking predicted by the empirical formula

The monotone relationship between these dimensionless parameters, indicates that the time scale of breaking can be predicted simply by empirical formula based on *Ir* and ζ. The predicted empirical formula for the linear fit is as follows:

$$T_p/(L_s/C_p) = -1.01\zeta + 0.35Ir + 1.96$$
$$T_p/T_c = 0.46\zeta + 0.17Ir + 0.46$$

Text S5. Previous work of energy distribution

Different methods of calculating energy distribution. Figure S8-S10 shows the relationship between the energy distribution and the blockage parameter, the modified degree of blocking ($B_m = B(a/h_1)^{\alpha_0}$, $\alpha_0 = 0.25$), the incident amplitude dimensionless by critical amplitude ($a/A_{c0}, A_{c0} \equiv \frac{1}{2}(h_2 - H_r - h_1) + \sqrt{h_1(h_2 - H_r)}$), respectively.

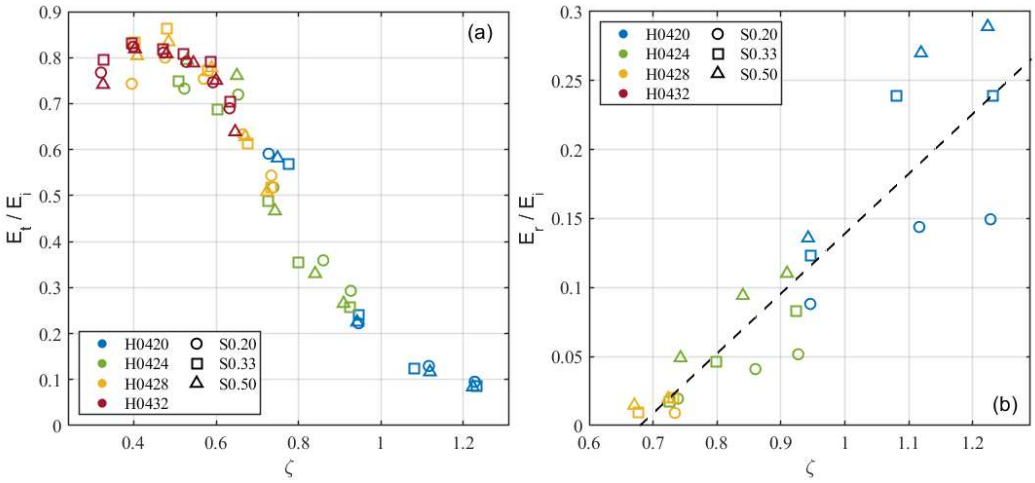

Figure S8. The relationship between blockage parameter ($\zeta = (a + h_1)/(h_1 + h_2 - H_r)$) and energy distribution. (a) transmission coefficient, (b) reflection coefficient. The dashed line in (b) shows a linear fit of the blockage parameter to the energy reflection coefficient, where $R = 0.43\zeta - 0.30$ and r^2=0.82. Blue, green, yellow and red indicate the upper and lower water depth ratios of 4:20, 4:24, 4:28 and 4:32 (the units are in cm), respectively. Triangles, squares and circles indicate the topographic slopes of 0.50, 0.33 and 0.20, respectively.

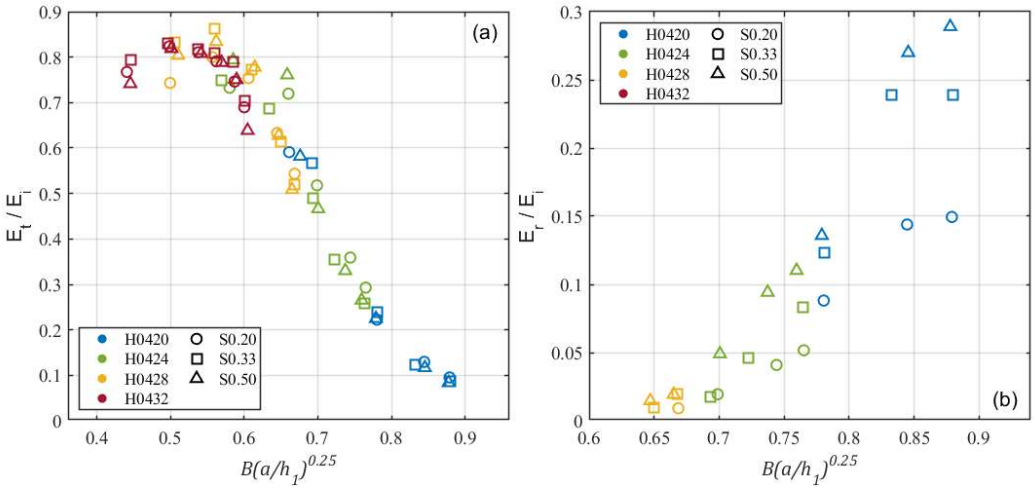

Figure S9. The relationship between modified degree of blocking ($B_m = B(a/h_1)^{\alpha_0}, \alpha_0 = 0.25$) and energy distribution. The legend is the same as in Figure S8.

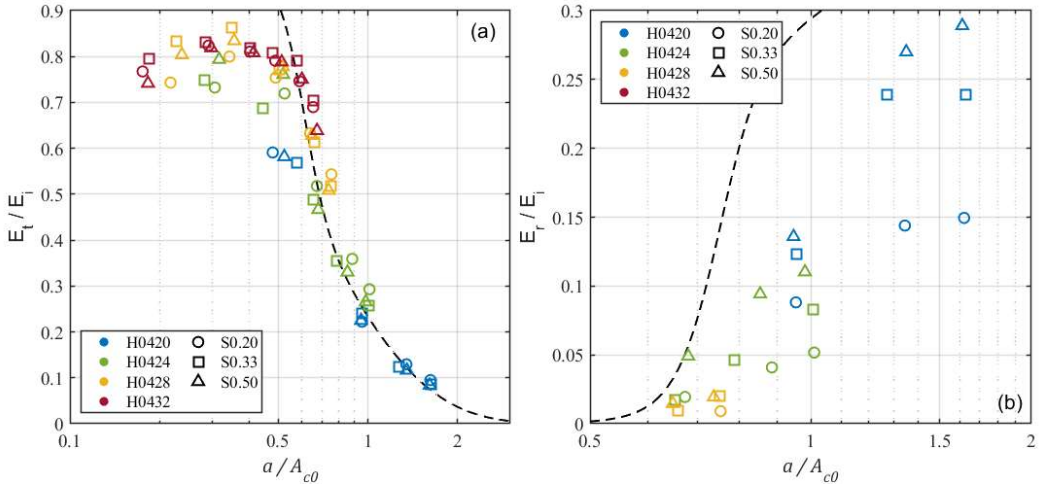

Figure S10. The relationship between the incident amplitude dimensionless by critical amplitude (a/A_{c0}, $A_{c0} \equiv \frac{1}{2}(h_2 - H_r - h_1) + \sqrt{h_1(h_2 - H_r)}$) and energy distribution. The legend is the same as in Figure S8. The fitting curves in (a) and (b) are Equation 5.1 and Equation 5.2 in Sutherland *et al.* (2015), respectively (Fitting results of numerical experiments at $s = 0.20$).